

# Enhancing Generalization and Plasticity for Sample Efficient Reinforcement Learning

Hoon Lee\* Hanseul Cho\* Hyunseung Kim\* Daehoon Gwak Joonkee Kim  
 Jaegul Choo Se-Young Yun Chulhee Yun  
 Kim Jaechul Graduate School of AI, KAIST  
 {joonleesky, jhs4015, mynsng, daehoon.gwak, joonkeekim,  
 jchoo, yunseyoung, chulhee.yun}@kaist.ac.kr

## Abstract

In Reinforcement Learning (RL), enhancing sample efficiency is crucial, particularly in scenarios when data acquisition is costly and risky. In principle, off-policy RL algorithms can improve sample efficiency by allowing multiple updates per environment interaction. However, these multiple updates often lead to overfitting, which decreases the network’s ability to adapt to new data. We conduct an empirical analysis of this challenge and find that generalizability and plasticity constitute different roles in improving the model’s adaptability. In response, we propose a combined usage of Sharpness-Aware Minimization (SAM) and a reset mechanism. SAM seeks wide, smooth minima, improving generalization, while the reset mechanism, through periodic reinitialization of the last few layers, consistently injects plasticity into the model. Through extensive empirical studies, we demonstrate that this combined usage improves sample efficiency and computational cost on the Atari-100k and DeepMind Control Suite benchmarks.

## 1 Introduction

The importance of sample efficiency in Reinforcement Learning (RL) lies in its potential to address computational and logistical issues associated with high sample complexity. It promotes RL’s practical utility in fields where data acquisition is constrained, costly, or risky, such as robotics, autonomous driving, and healthcare [33, 28]. In theory, off-policy RL algorithms [19, 15] can improve sample efficiency by multiple updates of policy or value functions, using identical data sample [34].

However, a key obstacle of these multiple updates is the model’s propensity to overfit to earlier interaction data, reducing its adaptability to future interactions [41, 11, 34]. In this paper, we analyze the model’s adaptability from two perspectives: *input adaptability* and *label adaptability*. First, as the agent continually interacts with the environment, adapting effectively when encountering new inputs is crucial. Second, in RL, the relationship between the input (i.e., observation) and the label (i.e., return or temporal difference target) continually changes. For instance, an action initially perceived as positive (i.e., high-reward) may later be valued as negative (i.e., low-reward) as more data becomes available. Therefore, the ability to adapt to the change of the label is important in RL [36, 45, 10, 41, 11].

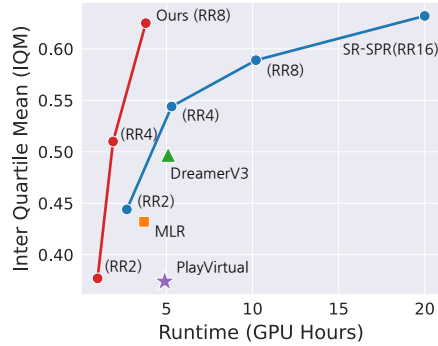


Figure 1: Scaling behavior of our method on Atari-100k benchmark, compared to the state-of-the-art methods. (see Section 5.3)

\*Equal contributions.

In this work, our investigation focuses on understanding the adaptability of the model to both inputs and labels. Specifically, we aim to understand how enhancing the model’s *generalizability* and *plasticity* influences its *input adaptability* and *label adaptability*, respectively. As a representative for improving the model’s generalization, we employ Sharpness-Aware Minimization (SAM [12]). SAM operates by seeking smooth and flat minima of the loss function during training, encouraging robustness of training and thus generalization [26]. As a representative for improving plasticity, we employ the reset mechanism [41]. This mechanism periodically reinitializes the last few layers of the network, which promotes plasticity and helps the model adapt to changing targets.

Through carefully designed synthetic experiments, we discovered that SAM primarily enhances the model’s input adaptation while having a limited impact on label adaptation. In contrast, the reset mechanism improves the model’s label adaptation while showing minimal influence on input adaptation. These findings suggest that generalization, facilitated by SAM, is closely tied to the model’s input adaptability, while plasticity, promoted by the reset mechanism, is more closely associated with label adaptability.

Building on these findings, our study demonstrates the effectiveness of combining Sharpness-Aware Minimization (SAM) and the reset mechanism to enhance a model’s generalization and plasticity simultaneously. We observe that integrating both methods generates a model with sparse feature extraction layers (the backbone) and dense prediction layers (the head). This structure aligns with the previous studies, suggesting that a sparse backbone (fewer active units) generally improves the model’s generalizability [12, 59, 18] and a dense head, characterized by a higher number of active units, has been linked to enhanced model plasticity [2, 10, 36]. Figure 1 indicates that our simple yet effective method substantially improves model plasticity, generalization, and sample efficiency with minimal computational overhead by not requiring architectural modification or integrating self-supervised learning objectives.

In summary, our main contributions are listed below:

- Through synthetic experiments, we find that incorporating both generalization and plasticity is crucial for improving the model’s ability to adapt to new data. (Section 4.)
- Through comprehensive empirical studies, we find that combining SAM for generalization and the reset mechanism for plasticity amplifies the sample efficiency that does not require any architectural modifications. (Section 5.2, 5.3.)
- We delve into implementation choices of how to apply SAM in the RL agent. (Section 5.4.)

## 2 Related Work

**Sample Efficient Reinforcement Learning.** Achieving sample efficiency is crucial for the successful application of reinforcement learning (RL) to real-world problems. Constraints such as limited online data collection (e.g., robotics, educational agents) or safety considerations (e.g., autonomous driving, healthcare) emphasize the need for efficient RL algorithms [28, 33]. Off-policy RL algorithms, such as Rainbow [19] and SAC [15] have shown potential in improving sample efficiency by enabling multiple updates to policy or value functions per data collection. Nonetheless, an increase in updates often induces overfitting, limiting the model’s adaptability to new datasets [21, 34].

To address overfitting by improving generalization, various approaches have been proposed. In pixel-based RL domains, data augmentation has proven effective in enhancing sample efficiency across discrete and continuous control environments [54, 53, 32, 42, 50]. Combining self-supervised auxiliary loss with data augmentation has also shown promise [31, 44]. In addition, regularization techniques such as L2 regularization [35], spectral normalization [14], and dropout [20] have been also introduced.

Parallel to the studies, another line of research has scrutinized the concept of plasticity in RL, which refers to the model’s ability to adapt to changing relationships between inputs and labels [36]. This adaptability is crucial in RL, where the model encounters dynamic shifts in these relationships as the policy and value functions evolve during training (e.g., an action initially perceived as positive may later be valued as negative as more data becomes available). The reduction in the number of active units in the network has been pinpointed as a crucial factor undermining this plasticity [2, 10]. To address this, strategies such as periodically reinitializing the last few layers [41, 11, 40, 46] or using Concatenated ReLU activation [45, 2] have been proposed. In addition, Lyle et al [36] discovered

that smoother gradients aid in preserving plasticity and introduced layer normalization after each convolutional and fully-connected layer which improves performance in Atari environments.

**Sharpness-Aware Optimization.** Generalization has been recognized as an important issue across the entirety of machine learning research, and numerous studies have been conducted to address it. Keskar et al. [26] propose a sharpness measure, arguing that finding wide and smooth minima is beneficial. Stochastic Weight Averaging (SWA) finds a flatter minimum by averaging checkpoints in the model’s training trajectory [22]. The work by [52] incorporates the addition of adversarial weight perturbation during training. These works are based on the hypothesis by [26] that wide and flat minima result in a more generalizable model.

Following a similar philosophy, Foret et al. [12] devised sharpness-aware minimization (SAM), which aims to reduce not only the value of the training loss but also its sharpness. In Section 3.2, we provide a detailed explanation of SAM. By reducing the sharpness of the loss and encouraging the model to get closer to a flat minimum, SAM has been successfully applied in various settings including computer vision [8], natural language processing [5], meta-learning [1], and model compression [39].

The aforementioned studies concern training in stationary data distributions. In contrast, our work involves experiments in reinforcement learning which has non-stationary data distribution in which the efficacy of SAM has not yet been verified. Indeed, we empirically verified that the usage of SAM enhances the generalizability and adaptability of deep RL agents.

### 3 Preliminaries

#### 3.1 Off-Policy Reinforcement Learning Algorithms

**Rainbow.** Rainbow [19] is a widely used off-policy algorithm for discrete control settings that integrates six different extensions to the standard DQN algorithm [38]. The extensions include Double Q-learning [48], Prioritized Experience Replay [43], Dueling Networks [51], Multi-Step Return, Distributional Q-function [6], and Noisy Networks [13]. These augmentations enhance the DQN’s performance and robustness, addressing shortcomings in function approximation and exploration-exploitation trade-offs.

The Q-value updates in the Rainbow algorithm follow the principle of minimizing the Temporal-Difference (TD) error which is defined as:

$$\mathcal{L}(\mathbf{w}, \mathbf{w}^-, \tau) = [Q_{\mathbf{w}}(s, a) - (r + \gamma \max_{a'} Q_{\mathbf{w}^-}(s', a'))]^2 \quad (1)$$

where  $\mathbf{w}$  denotes the model weights,  $\mathbf{w}^-$  is the weights of the target model, and  $\tau = (s, a, r, s')$  is the transition sampled from the replay buffer  $\mathcal{B}$ .

Noisy Networks [13] introduce stochasticity into the model weights, reparameterizing them as:

$$\mathbf{w} = \boldsymbol{\mu} + \boldsymbol{\sigma} \cdot \tilde{\boldsymbol{\epsilon}} \quad (2)$$

where  $\boldsymbol{\mu}$  and  $\boldsymbol{\sigma}$  are the learnable weights, whereas  $\tilde{\boldsymbol{\epsilon}}$  is a random vector sampled from an isotropic Gaussian distribution, adding randomness to the layer. (We denote element-wise product by ‘ $\cdot$ ’.)

**Soft Actor-Critic.** Soft Actor-Critic (SAC) [15], a prevalent off-policy algorithm for continuous control, aims to maximize the expected return coupled with an entropy bonus. SAC consists of a policy  $\pi$  and a critic model  $Q$ , each parameterized by weights  $\boldsymbol{\theta}$  and  $\mathbf{w}$  respectively.

In training, the critic  $Q_{\mathbf{w}}$  is trained to minimize the following objective, defined as

$$\mathcal{L}_Q(\boldsymbol{\theta}, \mathbf{w}; \tau) = [Q_{\mathbf{w}}(s, a) - (r + \gamma(Q_{\mathbf{w}}(s', a') - \alpha \log \pi_{\boldsymbol{\theta}}(s', a')))]^2, \quad a' \sim \pi_{\boldsymbol{\theta}}(\cdot | s') \quad (3)$$

where  $\alpha$  is the entropy coefficient and  $\tau = (s, a, r, s')$  is the transition sampled from the buffer  $\mathcal{B}$ .

Subsequently, the policy  $\pi_{\boldsymbol{\theta}}$  is jointly trained to maximize the following objective:

$$\mathcal{L}_{\pi}(\boldsymbol{\theta}, \mathbf{w}; s) = \mathbb{E}_{a \sim \pi_{\boldsymbol{\theta}}} [(Q_{\mathbf{w}}(s, a) - \alpha \log \pi_{\boldsymbol{\theta}}(a | s))]. \quad (4)$$

Unlike Rainbow, in SAC, SAM can be employed selectively on either the actor or the critic.

### 3.2 Sharpness-Aware Minimization on Replay Buffer

Here we elaborate on SAM adapted to an off-policy reinforcement learning setup. Originally, SAM aims to train a model which is robust to adversarially perturbed model weights, by solving the following bi-level optimization problem on the loss function  $\mathcal{L}$ :

$$\min_{\mathbf{w}} \{ \mathcal{L}^{\text{SAM}}(\mathbf{w}) := \max_{\epsilon: \|\epsilon\|_2 \leq \rho} \mathcal{L}(\mathbf{w} + \epsilon) \}. \quad (5)$$

This problem implies minimization of loss value around an  $\ell_2$ -ball of radius  $\rho$ , which encourages to Here,  $\rho > 0$  is a hyperparameter, called *SAM parameter*, restricting the size of perturbation to make the bi-level problem (5) feasible. Since the exact solution of the inner maximization problem in (5) is not tractable yet, first-order Taylor approximation is applied as a remedy for finding an approximately optimal perturbation  $\epsilon_\rho^*(\mathbf{w}) := \rho \nabla_{\mathbf{w}} \mathcal{L}(\mathbf{w}) / \|\nabla_{\mathbf{w}} \mathcal{L}(\mathbf{w})\|_2$  at  $\mathbf{w}$ . We call the step of computing  $\epsilon_\rho^*(\mathbf{w})$  as the *perturbation step* of SAM. As a result of the perturbation step, we can approximately solve the problem (5) with any gradient update algorithm (i.e., *base optimizer*), such as Stochastic Gradient Descent (SGD) or Adam [27], using the *SAM gradient* at current weight  $\mathbf{w}_t$ :  $\nabla_{\mathbf{w}} \mathcal{L}(\mathbf{w}_t + \epsilon_\rho^*(\mathbf{w}_t))$ . We call the step of updating the weights with SAM gradient as the *update step* of SAM. In essence, SAM is an iterative algorithm alternating perturbation and update steps. Readers can check a more detailed derivation of the SAM gradient in [12].

In off-policy RL, we never have access to the full static loss function as described above. Hence, analogous to most of the applications of SAM, it is natural to randomly sample a mini-batch  $\mathcal{B}_t$  of  $m$  transitions from replay buffer and apply SAM update (often called *m-SAM*) using the stochastic gradient  $\nabla_{\mathbf{w}} \mathcal{L}_{\mathcal{B}_t}(\mathbf{w}_t + \epsilon_{\rho, \mathcal{B}_t}^*(\mathbf{w}_t))$ , where  $\epsilon_{\rho, \mathcal{B}_t}^*(\mathbf{w}) := \rho \nabla_{\mathbf{w}} \mathcal{L}_{\mathcal{B}_t}(\mathbf{w}) / \|\nabla_{\mathbf{w}} \mathcal{L}_{\mathcal{B}_t}(\mathbf{w})\|_2$ .

There are several considerations for applying SAM to RL agents. When applying SAM to the Rainbow agent, the random noises from noisy layers embedded in the agent might hurt the SAM perturbation. However, we observe that the effect of regulating the noises is not significant. Moreover, there are options to apply SAM perturbation solely to the backbone or head. We find that applying SAM to the whole network is the most beneficial for enhancing generalization capability, yet we observe that solely applying SAM to the backbone is quite similar to the case of applying it to the whole. On the other hand, when applying SAM to the SAC agent, there are multiple loss functions to be optimized, which share parameters. Again, applying SAM to both actor and critic is the most desirable option, yet we observe that the application to critic is more critical for performance improvement. More detailed ablation studies appear in Section 5.4.

## 4 Synthetic Experiments on Supervised Learning

Understanding the impact of generalizability and plasticity on a model’s adaptability in Reinforcement Learning (RL) is a complex task due to RL’s multifaceted nature (e.g., credit assignments, noisy targets, exploration-exploitation tradeoff). To relieve this complexity, we designed synthetic supervised learning experiments within a controlled setting, utilizing the CIFAR-10 dataset [29]. We focused on two different adaptation scenarios to evaluate the model’s adaptation capabilities:

**Input Adaptation:** In RL, as the model continually interacts with the environment, it constantly encounters new sorts of data through exploration, and it must adapt effectively to it to make better decisions. To simulate this scenario, we partitioned the training data into 100 chunks, sequentially adding them to a buffer. The training was conducted by sampling data from this progressively growing buffer. If the model overfits to earlier data chunks and struggles to adapt to newer ones, it would suggest a degradation in performance compared to a model trained on the entire dataset.

**Label Adaptation:** In RL, relationships between the input and label can change. To replicate this condition, we designed a synthetic experiment with continuously changing labels. During training, labels were randomly altered 100 times, uniformly reassigning each class’s labels. Unlike a noisy label scenario, all data points within a class were consistently reassigned to a new class (e.g., all ‘cat’ images change from class 3 to class 4). If the model overfits to the earlier relationships, it would struggle to accurately map these transformed relationships.

For this experiment, we adopted a structure that reflects common architectural design in RL [38, 19, 54], consisting of three convolutional layers for the backbone and three fully-connected layers for the head. SGD with momentum is used, and the model is trained with over 50,000 updates with a batch size of 128. To ensure the model’s convergence, the last 10,000 updates were carried out without any shift with accuracy reported at the end of the training. To evaluate the effect of generalization, we

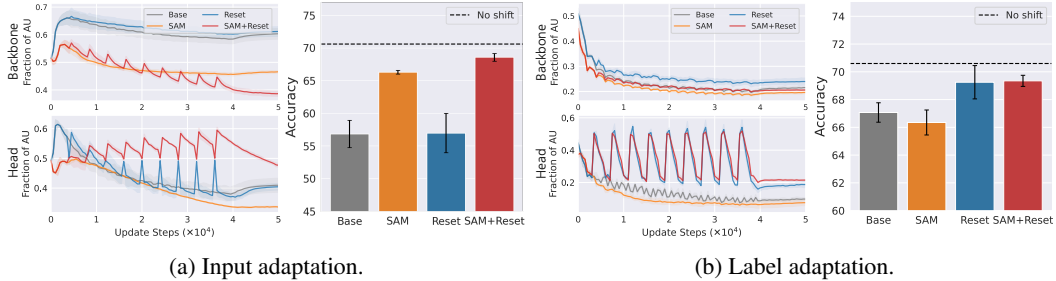


Figure 2: **Left.** The Input Adaptation experiment assesses the model’s adaptability to sequentially stacked data. The results highlight the importance of generalizability (SAM) for the input adaptation. **Right.** The Label Adaptation experiment assesses the model’s adaptability to the shifts in class labels. The outcomes emphasize the importance of plasticity (Reset) in label adaptation.

implemented Sharpness-Aware Minimization (SAM) and used the Reset mechanism to understand the impact of plasticity. Further details can be found in the Appendix.

Figure 2 summarizes the results of these experiments. Here, we discovered distinct benefits from employing Sharpness-Aware Minimization (SAM) and the Reset mechanism. SAM displayed its strength in enhancing the model’s input adaptability and promoting sparser features, as shown by a reduction in the active units of the model’s backbone. However, SAM’s contribution to enhancing label adaptability was less noticeable. In contrast, the Reset mechanism notably increased the model’s label adaptability, with an increase in active units in the model’s head. Nevertheless, the input adaptability enhancements from the Reset mechanism were less significant.

In conclusion, both generalizability, augmented by SAM, and plasticity, facilitated by the Reset mechanism, are important for model adaptability. Their combined presence is essential for effective adaptation in sample-efficient RL.

## 5 Experiments

In this study, we aim to scrutinize the effectiveness of the combined usage of SAM and Reset mechanism in reinforcement learning. We conduct experiments on two widely used benchmarks: Atari-100k [7] for discrete control and DeepMind Control Suite [47] for continuous control.

### 5.1 Experimental Setup

**Atari-100k.** Following the standard evaluation protocol from [24, 44], we evaluate the performance on 26 games limited to 100k interactions, where the results are averaged over 10 independent trials. We applied SAM optimizer on two different algorithms: Data-efficient Rainbow (DER) [49] and Data-Regularized Q-learning (DrQ) [54]. These algorithms are built on top of the Rainbow algorithm [19] where DER is a variant of Rainbow that optimizes its hyperparameters to achieve faster convergence during early stages, while DrQ utilizes data augmentation techniques to mitigate overfitting. Throughout all environments, we set the perturbation parameter  $\rho$  of SAM to 0.1.

**Deepmind Control Suite Medium (DMC-M).** To evaluate performance in the DMC benchmark, we adopt the evaluation protocol and network architecture described by Nikishin et al. [41]. This benchmark consists of 19 continuous control tasks (i.e., 8 easy tasks and 11 medium tasks), where the agent controls its behavior from raw pixels. We use 11 medium tasks and train for 2M environment steps. Within this setting, we apply the SAM optimizer to the Data-Regularized Q-learning (DrQ) algorithm [54], which incorporates data augmentation techniques in conjunction with the soft actor-critic algorithm [15]. For the quadruped environments, we set the perturbation parameter  $\rho$  to 0.1, while for the remaining environments, we use a value of 0.01.

**Baselines.** In this section, we present a selection of regularization methods designed to mitigate overfitting in RL. To enhance generalizability, we consider L2 regularization [35] which imposes a penalty on the weights of the parameters based on their Euclidean norm. We vary the regularization strength from  $\{0.001, 0.0001, 0.00001\}$ , selecting the model with the best performance.



For enhancing plasticity, we consider the resetting of the last few layers (Reset) [41], Concatenated ReLU (CReLU) [2], and Layer Normalization (LN) [36]. Reset involves periodically resetting the parameters of the head layers to their initial distribution. We reset the head layer’s parameters periodically after every 40,000 gradient updates for Atari and 100,000 gradient updates for DMC, following the original paper. For LN, we apply layer normalization directly after each convolutional and fully-connected layer. As for CReLU, we replace ReLU activation with concatenated ReLU, which preserves both positive and negative features.

**Metrics.** To gain a deeper understanding of the underlying geometry of the loss landscape, we employ two different metrics: the trace of the empirical Fisher matrix ( $\text{Tr}(F)$ ) [23], and the maximum eigenvalue of the Hessian ( $\lambda_{\max}$ ) [25]. These metrics provide insights into the curvature of the loss function, where a larger value indicates a sharper and more intricate optimization landscape, while a smaller value corresponds to a smoother and potentially more favorable landscape for optimization.

To quantify model plasticity, we periodically record the fraction of the active units in the feature map by forwarding 512 transitions [36, 45, 10]. When using ReLU activation, values below zero become inactive, which does not contribute to the updates of incoming weights.

To evaluate the performance of the agent, we report a bootstrapped interval for the interquartile mean (IQM), median, mean, and optimality gap, following the guidelines from [3]. For each environment within the Atari and DMC benchmarks, we calculate average end-of-training scores from 100 and 10 trajectories, respectively. For Atari, we normalize these scores to a Human Normalized Score (HNS) as  $\text{HNS} = \frac{\text{agent\_score} - \text{random\_score}}{\text{human\_score} - \text{random\_score}}$ , which quantifies the relative performance of the agent compared to human-level performance. More details of the experimental setup can be found in Appendix.

Table 1: **Performance on Atari-100k.** The results are averaged over 10 random seeds.

Algorithm	Method	$\text{Tr}(F)$ ( $10^{-4}$ )	$\lambda_{\max}$	IQM	Median	Mean
DER	Base	0.97	4.40	0.159 (0.143, 0.177)	0.175 (0.119, 0.204)	0.298 (0.274, 0.322)
	L2 [35]	0.96	16.84	0.210 (0.190, 0.236)	0.216 (0.162, 0.243)	0.375 (0.347, 0.407)
	SAM [12]	0.18	1.36	0.175 (0.154, 0.198)	0.210 (0.196, 0.272)	0.313 (0.399, 0.462)
	LN [36]	8.96	13.04	0.148 (0.132, 0.168)	0.171 (0.132, 0.188)	0.262 (0.246, 0.279)
	CReLU [2]	5.00	5.84	0.172 (0.156, 0.189)	0.149 (0.130, 0.180)	0.294 (0.268, 0.317)
	Reset [41]	1.42	11.39	0.202 (0.185, 0.222)	0.179 (0.153, 0.221)	0.366 (0.340, 0.394)
	SAM + Reset	0.15	1.72	<b>0.252</b> (0.230, 0.278)	<b>0.236</b> (0.195, 0.273)	<b>0.430</b> (0.400, 0.461)
DrQ	Base	5.54	16.07	0.258 (0.224, 0.292)	0.277 (0.209, 0.295)	0.476 (0.432, 0.520)
	L2 [35]	1.94	23.68	0.271 (0.227, 0.316)	0.268 (0.172, 0.358)	0.558 (0.492, 0.627)
	SAM [12]	0.42	2.12	0.325 (0.296, 0.354)	0.327 (0.284, 0.368)	0.501 (0.465, 0.537)
	LN [36]	11.76	10.98	0.259 (0.235, 0.293)	0.247 (0.218, 0.276)	0.463 (0.403, 0.522)
	CReLU [2]	4.46	20.50	0.256 (0.224, 0.287)	0.193 (0.176, 0.252)	0.498 (0.444, 0.553)
	Reset [41]	6.44	26.62	0.343 (0.314, 0.373)	0.291 (0.231, 0.369)	0.660 (0.611, 0.715)
	SAM + Reset	0.43	2.16	<b>0.411</b> (0.377, 0.447)	<b>0.374</b> (0.302, 0.458)	<b>0.753</b> (0.688, 0.836)

## 5.2 Main Experiment

In Table 1, we compare our method with other regularization baselines on Atari-100k. From the empirical results, we observed that combining SAM and Reset achieved superior performance compared to the other baselines. We believe that this can be attributed to SAM’s enhanced generalization capability achieved by smoother loss landscape and Reset’s ability to inject plasticity, as evidenced by our synthetic experiments. Empirically, we found that the synergy between the SAM and the reset mechanism was the best, which is illustrated in Section 5.4.

To further analyze performance improvement, we examined the number of active units of each algorithm in the backbone and head layers. From Figure 3, we observed that the algorithms with SAM decreased the number of active units in the backbone layers, and the algorithms with Reset increased the number of active units in the head layers. As we found in synthetic experiments, sparse features in the backbone layers tend to improve generalization ability, and dense features in head layers prevent loss of plasticity. Therefore, we speculate that the combination of SAM and Reset outperforms other methods by effectively improving generalization and plasticity simultaneously.

Table 2 summarizes the results of applying SAM to DMC benchmark. We found that SAM’s impact on performance improvement here is relatively small compared to Atari. In Atari, the agent is exposed

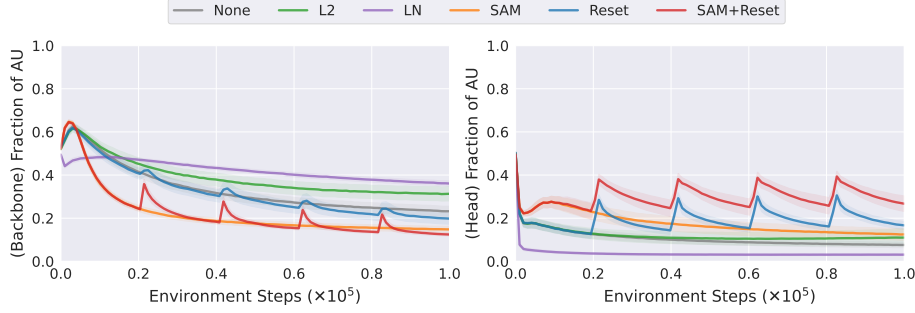


Figure 3: **Comparison of active units.** A Figure compares the fraction of active units for different regularization methods. We use DrQ architecture, evaluated on the Atari-100k benchmark. **Left:** The agent’s performance was inversely proportional to the fraction of active units on the backbone layers, where SAM+Reset outputs the sparsest feature. **Right:** The agent’s performance was proportional to the fraction of active units on the head layers, where SAM+Reset outputs the densest feature.

to a diverse range of visual inputs as it progresses through different stages or game screens. However, the DMC environments feature a fixed camera and background, with the agent navigating within this limited visual context. This reduced visual variety in DMC may explain the relatively modest impact of SAM on performance, as its main focus is enhancing generalization to new visual inputs.

In contrast, we observed substantial benefits from plasticity improvement methods such as Layer Normalization (LN), Concatenated ReLU (CReLU), and Reset. In DMC, the primary challenge lies in label adaptation rather than input adaptation. For example, in the cheetah environment, initially moving backward may seem advantageous, but the model learns over time that running forward yields greater rewards. This indicates the importance of improving plasticity in DMC benchmarks.

Table 2: **Performance on DMC-M benchmark.** For the base algorithm (DrQ) and the Reset, we adopt the results from [41].

Method	IQM	Median	Mean
Base	213 (146, 304)	288 (223, 356)	293 (239, 347)
L2 [35]	149 (082, 237)	238 (189, 321)	257 (201, 315)
SAM [12]	278 (196, 371)	341 (264, 404)	332 (277, 389)
LN [36]	412 (332, 488)	415 (351, 491)	421 (366, 477)
CReLU [2]	338 (227, 457)	398 (312, 477)	394 (329, 462)
Reset [41]	514 (434, 590)	491 (430, 568)	498 (442, 555)
<b>SAM + Reset</b>	<b>519</b> (442, 594)	<b>511</b> (437, 574)	<b>506</b> (450, 561)

### 5.3 Comparison to the State-of-the-art Methods

Here we present a comparison of our simple yet effective methodology against various state-of-the-art (SOTA) model-based and model-free methods, evaluated on the Atari-100k benchmarks. Our approach was developed by simply incorporating Sharpness-Aware Minimization (SAM), reset mechanism, and Shrink & Perturb [4] into the DrQ algorithm. Shrink & Perturb softly reinitializes the model’s parameters as  $\theta^t = \alpha\theta^{t-1} + (1 - \alpha)\phi$ , where  $\phi \sim \text{initializer}$ . Aligning with the strategy of D’Oro et al. [11], we employ  $\alpha = 0.8$  and apply Shrink & Perturb to the backbone network’s parameters during every reset, aiming to boost the plasticity of the model’s backbone. While this adjustment slightly lowers performance at a replay ratio of 2, it substantially enhances performance as we scale up the replay ratio in our method.

In conducting our evaluations and computing the GPU hours for each method, we utilized their official code and calculated the time based on the average time for each run. Notably, PlayVirtual [56], MLR [57], SR-SPR [11], and our own approach can parallelize multiple runs on a single GPU. Thus, for a fair comparison, we followed the protocol as outlined by [11], dividing the total execution time by the number of runs. All methods, including ours, were implemented using the PyTorch framework. DreamerV3 [16] was the only exception, using the JAX framework. Here, it is important to note that, due to the just-in-time compilation method from JAX, we found it to be approximately 1.5-2x faster than PyTorch. Thus, DreamerV3 may require around 1.5-2x longer computation time when implemented in a PyTorch framework.

Table 3 demonstrates the effectiveness of our approach. Our method and SR-SPR construct a Pareto frontier for Inter-Quartile Mean (IQM) and Optimality Gap (OG) relative to computational cost which implies effective computational efficiency. While EfficientZero demonstrates state-of-the-art

Table 3: **Comparison to the SOTA on Atari-100k.** For IRIS, DreamerV3, EfficientZero, and PlayVirtual, MLR, SR-SPR, the results are averaged over 5, 5, 32, and 15, 3, 10 seeds respectively. For our method, the results are averaged over 5 random seeds. The GPU hours for DreamerV3<sup>†</sup> are calculated based on their JAX implementation.

Type	Method	Search	Params (M)	RR	GPU hours	IQM	Median	Mean	OG
Model-Based	IRIS [37]	-	30.4	-	36.3	0.501	0.289	1.046	0.512
	DreamerV3 [16]	-	17.9	-	5.1 <sup>†</sup>	0.497	0.466	1.097	0.505
	EfficientZero [55]	✓	8.4	-	28.0	n/a	1.090	1.943	n/a
	PlayVirtual [56]	-	7.4	2	4.9	0.374	n/a	n/a	0.558
	MLR [57]	-	161.7	2	3.7	0.432	n/a	n/a	0.522
Model-Free	SR-SPR [11]	-	7.3	2	2.7	0.444	0.336	0.910	0.516
				4	5.3	0.544	0.523	1.111	0.470
				8	10.2	0.589	0.560	1.188	0.452
				16	20.0	0.632	0.685	1.272	0.433
	Ours	-	6.8	2	1.0	0.377	0.281	0.764	0.554
				4	1.9	0.510	0.459	0.923	0.486
				8	3.8	0.625	0.544	1.008	0.442

performance in terms of Median and Mean scores, it is the only variant that utilized a search algorithm and a domain-specific heuristic (early environment resets). Setting these specific elements aside, our method emerges as a compelling contender against the other methods.

In conclusion, our simple method substantially improves model plasticity, generalization, and sample efficiency with minimal computational overhead. It demonstrates robust competitiveness, even without integrating self-supervised learning objectives. Future research could further enhance our method’s generalization ability, perhaps by adopting self-supervised objectives as seen in PlayVirtual [56], MLR [57], and SR-SPR [11]. This highlights the promising avenue of enhancing generalization and plasticity to improve sample efficiency in Reinforcement Learning.

#### 5.4 Ablation Studies

We conduct some ablation studies aiming to answer the following four questions: (1) Are there other synergistic combinations apart from SAM and reset? (2) How should we deal with *noisy layers* during training? (3) What if we solely apply SAM perturbation to the *backbone* or *head* of Rainbow agent? (4) Lastly, what if we solely apply SAM perturbation to the *actor* or *critic* of SAC agent? Every question is answered by experiments with the DrQ algorithm tested on the Atari-100k benchmark, except for the last question that we test on the DMC-M benchmark with the SAC agent.

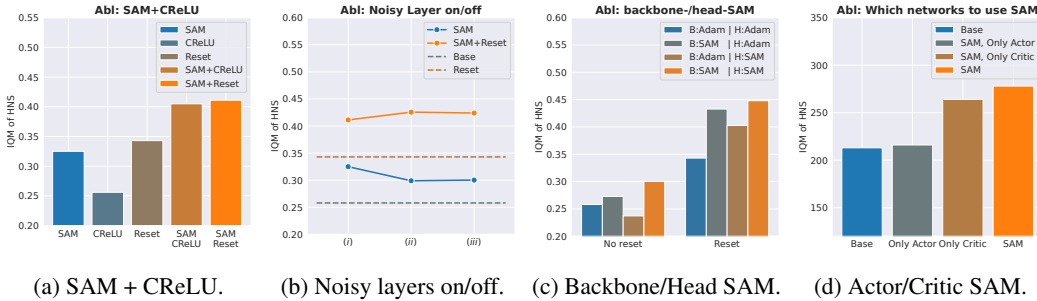


Figure 4: **Ablation study.** Details are in Section 5.4.

**SAM + CReLU.** Here we further explored the effectiveness of different synergies to enhance the generalization and plasticity of our reinforcement learning model. Specifically, we investigated the combination of SAM, employed for its generalization capabilities, and CReLU activation, known for enhancing plasticity. Our results demonstrate that the SAM + CReLU combination performs competitively with our proposed SAM + reset strategy. This finding underscores the central message of our work: it is important to address both generalizability and plasticity for improving sample efficiency in RL algorithms.



**Noisy Layers.** For the case of the Rainbow agent, we compare three different schemes of SAM updates regarding random noises from noisy layers: (i) perturbation with independent noise, using independently sampled (*e.g.*, different) noise between perturbation and update step (default setting); (ii) update with reused noise, turning the noise on at the perturbation step and reusing that noise at the update step; (iii) noise-less perturbation, turning the noise off at the perturbation step and turning it on at the update step. Despite the variations, the overall impact on the agent’s performance was relatively consistent. Note that option (i) is the most naïve approach which can be implemented by simply adding a SAM optimizer code block into any RL implementation with noisy layers.

**Backbone-SAM v.s. Head-SAM.** We experiment with resectioning the parts to be updated with SAM in the RL agent architecture. We temporarily turn off the gradient of either backbone or head at the perturbation step and then turn on that gradient back at the update step. The result of the experiment, presented in Figure 4c, says that updating with backbone-only perturbation is more beneficial than using head-only perturbation, although applying both is much better. Indeed, SAM perturbation of the head alone hurts the performance without any other SAM perturbation or resetting.

We want to explain why these happen from the point of view of the number of active neurons in the backbone/head. Interestingly, we observe that the SAM perturbation of backbone parameters induces *more* active units in the head, whereas the SAM perturbation of head parameters results in *less* active units in the backbone. Recall that both tendencies are observed when we apply SAM perturbation to both the backbone and head at once. From this, we can say that the rise of active units in the head by applying SAM is due to the SAM perturbation of the backbone, whereas the reason for the backbone getting sparser is the SAM perturbation of the head.

**Actor-SAM v.s. Critic-SAM.** SAC is an actor-critic algorithm that employs three distinct sets of updating parameters, namely the actor, critic, and alpha. Since alpha has just one parameter, we focus on investigating the impact of SAM on actor and critic parameters. We conduct an ablation study utilizing the identical configuration as the DMC experiment presented in Section 5.2. Figure 4d demonstrates that exclusively applying SAM to critic parameters is more critical than solely applying SAM to actor parameters while using both is much better.

In the context of SAC, the actor and critic networks are constructed to jointly utilize the backbone layer. In order to ensure stable learning, updates to the backbone layer are exclusively driven by critic losses, while actor losses do not influence the backbone layer [54, 53]. Consequently, if SAM is exclusively applied to the actor parameters, the backbone layer remains unaffected by SAM as there is no gradient propagation. As a result, the performance of the SAM solely used on the actor parameters, which has no impact on the backbone, is inferior to other approaches incorporating SAM, which corroborates the aforementioned findings.

## 6 Conclusion, Limitations, and Future Work

In this work, we dissect the roles of generalization and plasticity in Reinforcement Learning, revealing their critical importance. We introduce a novel, easily-integrable strategy that combines SAM optimizer [12] and a reset mechanism [41], requiring no architectural modifications to existing algorithms. This strategy significantly enhances generalizability and fosters plasticity, leading to marked improvements in sample efficiency.

However, our work has several limitations. First, there is a need for further exploration to understand the diverse synergetic relationships among different types of algorithms that enhance generalization and plasticity. Second, our approach has not been validated in model-based algorithms with state-of-the-art sample efficiency [55, 17]. Yet we remain optimistic about its potential for improvement. Lastly, our experiments have been confined to the Atari and DMC environments. An intriguing next step would be to explore our approach’s performance in more complex environments like MetaWorld [58], or Procgen [9], which demand higher levels of generalizability.

Despite these limitations, our work provides practical insights into enhancing the adaptability of RL agents. We hope our findings open up a diverse possibility for future exploration, potentially leading to more sample-efficient and adaptable algorithms in RL.

## Acknowledgments and Disclosure of Funding

This work was supported by the Institute of Information & communications Technology Planning & Evaluation (IITP) grant funded by the Korea government(MSIT) (No.2019-0-00075, Artificial Intelligence Graduate School Program(KAIST)).

## References

- [1] Momin Abbas, Quan Xiao, Lisha Chen, Pin-Yu Chen, and Tianyi Chen. Sharp-maml: Sharpness-aware model-agnostic meta learning. In *Proc. the International Conference on Machine Learning (ICML)*, 2022. 3
- [2] Zaheer Abbas, Rosie Zhao, Joseph Modayil, Adam White, and Marlos C Machado. Loss of plasticity in continual deep reinforcement learning. *arXiv preprint arXiv:2303.07507*, 2023. 2, 6, 7
- [3] Rishabh Agarwal, Max Schwarzer, Pablo Samuel Castro, Aaron C Courville, and Marc Bellemare. Deep reinforcement learning at the edge of the statistical precipice. *Proc. the Advances in Neural Information Processing Systems (NeurIPS)*, 34:29304–29320, 2021. 6
- [4] Jordan Ash and Ryan P Adams. On warm-starting neural network training. *Proc. the Advances in Neural Information Processing Systems (NeurIPS)*, 33:3884–3894, 2020. 7
- [5] Dara Bahri, Hossein Mobahi, and Yi Tay. Sharpness-aware minimization improves language model generalization. In *Proc. the Annual Meeting of the Association for Computational Linguistics (ACL)*, pages 7360–7371, 2022. 3
- [6] Marc G Bellemare, Will Dabney, and Rémi Munos. A distributional perspective on reinforcement learning. In *Proc. the International Conference on Machine Learning (ICML)*, pages 449–458. PMLR, 2017. 3
- [7] Marc G Bellemare, Yavar Naddaf, Joel Veness, and Michael Bowling. The arcade learning environment: An evaluation platform for general agents. *Journal of Artificial Intelligence Research*, 47:253–279, 2013. 5
- [8] Xiangning Chen, Cho-Jui Hsieh, and Boqing Gong. When vision transformers outperform resnets without pre-training or strong data augmentations. In *International Conference on Learning Representations*, 2022. 3
- [9] Karl Cobbe, Chris Hesse, Jacob Hilton, and John Schulman. Leveraging procedural generation to benchmark reinforcement learning. In *Proc. the International Conference on Machine Learning (ICML)*, pages 2048–2056. PMLR, 2020. 9
- [10] Shibhansh Dohare, Richard S Sutton, and A Rupam Mahmood. Continual backprop: Stochastic gradient descent with persistent randomness. *arXiv preprint arXiv:2108.06325*, 2021. 1, 2, 6
- [11] Pierluca D’Oro, Max Schwarzer, Evgenii Nikishin, Pierre-Luc Bacon, Marc G Bellemare, and Aaron Courville. Sample-efficient reinforcement learning by breaking the replay ratio barrier. In *The Eleventh International Conference on Learning Representations*, 2023. 1, 2, 7, 8, 14
- [12] Pierre Foret, Ariel Kleiner, Hossein Mobahi, and Behnam Neyshabur. Sharpness-aware minimization for efficiently improving generalization. In *Proc. the International Conference on Learning Representations (ICLR)*, 2021. 2, 3, 4, 6, 7, 9
- [13] Meire Fortunato, Mohammad Gheshlaghi Azar, Bilal Piot, Jacob Menick, Ian Osband, Alex Graves, Vlad Mnih, Remi Munos, Demis Hassabis, Olivier Pietquin, et al. Noisy networks for exploration. *arXiv preprint arXiv:1706.10295*, 2017. 3
- [14] Florin Gogianu, Tudor Berariu, Mihaela C Rosca, Claudia Clopath, Lucian Busoniu, and Razvan Pascanu. Spectral normalisation for deep reinforcement learning: an optimisation perspective. In *International Conference on Machine Learning*, pages 3734–3744. PMLR, 2021. 2

- [15] Tuomas Haarnoja, Aurick Zhou, Pieter Abbeel, and Sergey Levine. Soft actor-critic: Off-policy maximum entropy deep reinforcement learning with a stochastic actor. In *Proc. the International Conference on Machine Learning (ICML)*, pages 1861–1870. PMLR, 2018. 1, 2, 3, 5
- [16] Danijar Hafner, Jurgis Pasukonis, Jimmy Ba, and Timothy Lillicrap. Mastering diverse domains through world models. *arXiv preprint arXiv:2301.04104*, 2023. 7, 8
- [17] Danijar Hafner, Jurgis Pasukonis, Jimmy Ba, and Timothy Lillicrap. Mastering diverse domains through world models. *arXiv preprint arXiv:2301.04104*, 2023. 9
- [18] Abolfazl Hashemi, Hayden Schaeffer, Robert Shi, Ufuk Topcu, Giang Tran, and Rachel Ward. Generalization bounds for sparse random feature expansions. *arXiv preprint arXiv:2103.03191*, 2021. 2
- [19] Matteo Hessel, Joseph Modayil, Hado Van Hasselt, Tom Schaul, Georg Ostrovski, Will Dabney, Dan Horgan, Bilal Piot, Mohammad Azar, and David Silver. Rainbow: Combining improvements in deep reinforcement learning. In *Proc. the AAAI Conference on Artificial Intelligence (AAAI)*, 2018. 1, 2, 3, 4, 5, 14
- [20] Takuya Hiraoka, Takahisa Imagawa, Taisei Hashimoto, Takashi Onishi, and Yoshimasa Tsuruoka. Dropout q-functions for doubly efficient reinforcement learning. *Proc. the International Conference on Learning Representations (ICLR)*, 2022. 2
- [21] Maximilian Igl, Gregory Farquhar, Jelena Luketina, Wendelin Boehmer, and Shimon Whiteson. Transient non-stationarity and generalisation in deep reinforcement learning. *Proc. the International Conference on Learning Representations (ICLR)*, 2021. 2
- [22] Pavel Izmailov, Dmitrii Podoprikin, T. Garipov, Dmitry P. Vetrov, and Andrew Gordon Wilson. Averaging weights leads to wider optima and better generalization. In *Proc. the Conference on Uncertainty in Artificial Intelligence (UAI)*, 2018. 3, 19
- [23] Stanislaw Jastrzebski, Devansh Arpit, Oliver Astrand, Giancarlo B Kerg, Huan Wang, Caiming Xiong, Richard Socher, Kyunghyun Cho, and Krzysztof J Geras. Catastrophic fisher explosion: Early phase fisher matrix impacts generalization. In *Proc. the International Conference on Machine Learning (ICML)*, pages 4772–4784. PMLR, 2021. 6
- [24] Łukasz Kaiser, Mohammad Babaeizadeh, Piotr Miłoś, Błażej Osipiński, Roy H Campbell, Konrad Czechowski, Dumitru Erhan, Chelsea Finn, Piotr Kozakowski, Sergey Levine, et al. Model based reinforcement learning for atari. In *Proc. the International Conference on Learning Representations (ICLR)*, 2019. 5
- [25] Simran Kaur, Jeremy Cohen, and Zachary Chase Lipton. On the maximum hessian eigenvalue and generalization. In *I Can’t Believe It’s Not Better Workshop: Understanding Deep Learning Through Empirical Falsification*, 2023. 6
- [26] Nitish Shirish Keskar, Dheevatsa Mudigere, Jorge Nocedal, Mikhail Smelyanskiy, and Ping Tak Peter Tang. On large-batch training for deep learning: Generalization gap and sharp minima. In *Proc. the International Conference on Learning Representations (ICLR)*, 2017. 2, 3
- [27] Diederik P Kingma and Jimmy Ba. Adam: A method for stochastic optimization. *Proc. the International Conference on Learning Representations (ICLR)*, 2015. 4
- [28] Jens Kober, J Andrew Bagnell, and Jan Peters. Reinforcement learning in robotics: A survey. *The International Journal of Robotics Research*, 2013. 1, 2
- [29] Alex Krizhevsky, Geoffrey Hinton, et al. Learning multiple layers of features from tiny images. *Toronto, ON, Canada*, 2009. 4
- [30] Alex Krizhevsky, Geoffrey Hinton, et al. Learning multiple layers of features from tiny images. *Toronto, ON, Canada*, 2009. 14
- [31] Michael Laskin, Aravind Srinivas, and Pieter Abbeel. Curl: Contrastive unsupervised representations for reinforcement learning. In *Proc. the International Conference on Machine Learning (ICML)*, 2020. 2

- [32] Misha Laskin, Kimin Lee, Adam Stooke, Lerrel Pinto, Pieter Abbeel, and Aravind Srinivas. Reinforcement learning with augmented data. *Proc. the Advances in Neural Information Processing Systems (NeurIPS)*, 2020. 2
- [33] Sergey Levine, Aviral Kumar, George Tucker, and Justin Fu. Offline reinforcement learning: Tutorial, review, and perspectives on open problems. *arXiv preprint arXiv:2005.01643*, 2020. 1, 2
- [34] Qiyang Li, Aviral Kumar, Ilya Kostrikov, and Sergey Levine. Efficient deep reinforcement learning requires regulating overfitting. *arXiv preprint arXiv:2304.10466*, 2023. 1, 2
- [35] Zhuang Liu, Xuanlin Li, Bingyi Kang, and Trevor Darrell. Regularization matters in policy optimization—an empirical study on continuous control. *Proc. the International Conference on Learning Representations (ICLR)*, 2021. 2, 5, 6, 7
- [36] Clare Lyle, Zeyu Zheng, Evgenii Nikishin, Bernardo Avila Pires, Razvan Pascanu, and Will Dabney. Understanding plasticity in neural networks. *Proc. the International Conference on Machine Learning (ICML)*, 2023. 1, 2, 6, 7
- [37] Vincent Micheli, Eloi Alonso, and François Fleuret. Transformers are sample efficient world models. *arXiv preprint arXiv:2209.00588*, 2022. 8
- [38] Volodymyr Mnih, Koray Kavukcuoglu, David Silver, Andrei A Rusu, Joel Veness, Marc G Bellemare, Alex Graves, Martin Riedmiller, Andreas K Fidjeland, Georg Ostrovski, et al. Human-level control through deep reinforcement learning. *Nature*, 2015. 3, 4, 14
- [39] Clara Na, Sanket Vaibhav Mehta, and Emma Strubell. Train flat, then compress: Sharpness-aware minimization learns more compressible models. In *Proc. of the Conference on Empirical Methods in Natural Language Processing (EMNLP)*, pages 4909–4936, 2022. 3
- [40] Evgenii Nikishin, Junhyuk Oh, Georg Ostrovski, Clare Lyle, Razvan Pascanu, Will Dabney, and André Barreto. Deep reinforcement learning with plasticity injection. *arXiv preprint arXiv:2305.15555*, 2023. 2
- [41] Evgenii Nikishin, Max Schwarzer, Pierluca D’Oro, Pierre-Luc Bacon, and Aaron Courville. The primacy bias in deep reinforcement learning. In *Proc. the International Conference on Machine Learning (ICML)*, pages 16828–16847. PMLR, 2022. 1, 2, 5, 6, 7, 9, 14, 15, 19
- [42] Roberta Raileanu, Max Goldstein, Denis Yarats, Ilya Kostrikov, and Rob Fergus. Automatic data augmentation for generalization in deep reinforcement learning. *arXiv preprint arXiv:2006.12862*, 2020. 2
- [43] Tom Schaul, John Quan, Ioannis Antonoglou, and David Silver. Prioritized experience replay. *Proc. the International Conference on Learning Representations (ICLR)*, 2016. 3
- [44] Max Schwarzer, Ankesh Anand, Rishab Goel, R Devon Hjelm, Aaron Courville, and Philip Bachman. Data-efficient reinforcement learning with self-predictive representations. In *Proc. the International Conference on Learning Representations (ICLR)*, 2020. 2, 5
- [45] Wenling Shang, Kihyuk Sohn, Diogo Almeida, and Honglak Lee. Understanding and improving convolutional neural networks via concatenated rectified linear units. In *Proc. the International Conference on Machine Learning (ICML)*, pages 2217–2225. PMLR, 2016. 1, 2, 6
- [46] Ghada Sokar, Rishabh Agarwal, Pablo Samuel Castro, and Utku Evci. The dormant neuron phenomenon in deep reinforcement learning. *arXiv preprint arXiv:2302.12902*, 2023. 2
- [47] Yuval Tassa, Yotam Doron, Alistair Muldal, Tom Erez, Yazhe Li, Diego de Las Casas, David Budden, Abbas Abdolmaleki, Josh Merel, Andrew LeFrancq, et al. Deepmind control suite. *arXiv preprint arXiv:1801.00690*, 2018. 5
- [48] Hado Van Hasselt, Arthur Guez, and David Silver. Deep reinforcement learning with double q-learning. In *Proc. the AAAI Conference on Artificial Intelligence (AAAI)*, volume 30, 2016. 3

- [49] Hado P Van Hasselt, Matteo Hessel, and John Aslanides. When to use parametric models in reinforcement learning? *Proc. the Advances in Neural Information Processing Systems (NeurIPS)*, 32, 2019. 5, 14
- [50] Kaixin Wang, Bingyi Kang, Jie Shao, and Jiashi Feng. Improving generalization in reinforcement learning with mixture regularization. *Proc. the Advances in Neural Information Processing Systems (NeurIPS)*, 33:7968–7978, 2020. 2
- [51] Ziyu Wang, Tom Schaul, Matteo Hessel, Hado Hasselt, Marc Lanctot, and Nando Freitas. Dueling network architectures for deep reinforcement learning. In *Proc. the International Conference on Machine Learning (ICML)*, pages 1995–2003. PMLR, 2016. 3
- [52] Dongxian Wu, Shu-Tao Xia, and Yisen Wang. Adversarial weight perturbation helps robust generalization. *Advances in Neural Information Processing Systems*, 33:2958–2969, 2020. 3
- [53] Denis Yarats, Rob Fergus, Alessandro Lazaric, and Lerrel Pinto. Mastering visual continuous control: Improved data-augmented reinforcement learning. *arXiv preprint arXiv:2107.09645*, 2021. 2, 9
- [54] Denis Yarats, Ilya Kostrikov, and Rob Fergus. Image augmentation is all you need: Regularizing deep reinforcement learning from pixels. In *Proc. the International Conference on Machine Learning (ICML)*, 2020. 2, 4, 5, 9, 14
- [55] Weirui Ye, Shaohuai Liu, Thanard Kurutach, Pieter Abbeel, and Yang Gao. Mastering atari games with limited data. *Proc. the Advances in Neural Information Processing Systems (NeurIPS)*, 34:25476–25488, 2021. 8, 9
- [56] Tao Yu, Cuiling Lan, Wenjun Zeng, Mingxiao Feng, Zhizheng Zhang, and Zhibo Chen. Playvirtual: Augmenting cycle-consistent virtual trajectories for reinforcement learning. *Proc. the Advances in Neural Information Processing Systems (NeurIPS)*, 34:5276–5289, 2021. 7, 8
- [57] Tao Yu, Zhizheng Zhang, Cuiling Lan, Yan Lu, and Zhibo Chen. Mask-based latent reconstruction for reinforcement learning. *Proc. the Advances in Neural Information Processing Systems (NeurIPS)*, 35:25117–25131, 2022. 7, 8
- [58] Tianhe Yu, Deirdre Quillen, Zhanpeng He, Ryan Julian, Karol Hausman, Chelsea Finn, and Sergey Levine. Meta-world: A benchmark and evaluation for multi-task and meta reinforcement learning. In *Conference on robot learning*, pages 1094–1100. PMLR, 2020. 9
- [59] Xiong Zhou, Xianming Liu, Chenyang Wang, Deming Zhai, Junjun Jiang, and Xiangyang Ji. Learning with noisy labels via sparse regularization. In *Proceedings of the IEEE/CVF International Conference on Computer Vision*, pages 72–81, 2021. 2



## 7 Implementation Details

### 7.1 Computation

For all experiments, we used an NVIDIA RTX 3090 GPU for neural computations and a 32-core AMD EPYC 7502 for multi-threaded tasks, accelerating machine learning model training and inference.

For the Atari 100k benchmark, our computations were based on the DrQ algorithm with SAM (Sharpness-Aware Minimization) and Reset, using a replay ratio of 2. We ran 3 experiments in parallel on a single GPU, all completing within 3 hours, which effectively translates to an average of 1 hour per run.

Regarding the DeepMind Control Suite (DMC), runtimes varied based on the specific environment due to the differences in action repeat (i.e., ). On the NVIDIA RTX 3090 GPU, our setup took roughly 8 hours to complete 2 million environment steps with an action repeat of 4, and around 15 hours with an action repeat of 2.

### 7.2 Synthetic Experiment

In our synthetic experiment, we utilized the CIFAR-10 dataset [30] to test both input adaptation and label adaptation scenarios. The dataset comprises 50,000 training images and 10,000 test images, evenly distributed across 10 classes. Each image in the dataset is a color image of size 32x32.

**Input Adaptation:** In the input adaptation experiment, the training data was segmented into 100 chunks, each consisting of 500 images. These chunks were sequentially added to a buffer, which progressively expanded during the course of the experiment. For every model update, data were randomly sampled from this progressively growing buffer.

**Label Adaptation:** In the label adaptation experiment, label alterations were done 100 times during the training phase. The process of label reassignment was performed in a uniform manner across all classes. For example, if the original class labels ranged from 0 to 9, after each label alteration, all data points within a specific class would be consistently reassigned to a new class within the same range.

We selected a model architecture that reflects common architectural designs utilized in reinforcement learning research [38, 19]. The architecture consists of three convolutional layers for the backbone and three fully-connected layers for the head. The three convolutional layers employed kernel sizes of 3x3, with strides of (3, 3, 1), and the number of channels was set as (32, 64, 64) respectively. Subsequent to this, the three fully-connected layers consisted of hidden dimensions of (512, 128, 10).

The model was trained for a total of 50,000 updates, with a batch size of 128 for each update (i.e., equivalent to training 128 epochs). The last 10,000 updates were performed without any input or label alterations to ensure that the model reached convergence. The training was conducted using Stochastic Gradient Descent (SGD) with momentum. To select the learning rates and weight decay rates, we vary the values range from  $\{0.1, 0.01, 0.001\}$  and  $\{0.001, 0.0001, 0.00001\}$ , respectively. For the input adaptation experiment, we used a learning rate of 0.001 and a weight decay of 0.0001, whereas, for the label adaptation experiment, we employed a learning rate of 0.01 and a weight decay of 0.0001.

To induce generalization in the model, we implemented Sharpness-Aware Minimization (SAM) and Reset mechanisms. For SAM, we set the  $\rho$  to 0.1. In the case of Reset, we periodically reinitialized the head (i.e., the fully connected layers) at every alternation step.

Finally, we reported the test accuracy, averaged over 5 random seeds, at the end of each experiment.

### 7.3 Arcade Learning Environment (Atari-100k)

We implemented the Rainbow algorithm [19] while following design choices from DER [49] and DrQ [54]. Furthermore, we integrated modifications suggested by D’Oro et al [11], including the application of a momentum encoder for the target network and the use of this target network for exploration. While these adjustments had little impact under a low replay ratio regime ( $\leq 2$ ), they played a significant role when scaling the replay ratio with the reset mechanism [41]. A detailed hyperparameter is described in Table 4.

For L2 regularization, we vary the regularization strength from  $\{0.001, 0.0001, 0.00001\}$ , selecting the model with the best performance. In the case of LN, we apply layer normalization after each convolutional and fully-connected layer. For CReLU, we replaced all ReLU activations with concatenated ReLU. For the methods using the Reset mechanism, we reset the head layer’s parameters every 40,000 gradient updates, in accordance with the original paper [41].

Table 4: **Hyperparameters on Atari 100k.** The ones introduced by this work are at the bottom.

Hyperparameter	Value
State downsample size	(84, 84)
Grey scaling	True
Data augmentation	Random Shifts and Intensity Jittering
Random Shifts	$\pm 4$ pixels
Intensity Jittering scale	0.05
Frame skip	4
Stacked frames	4
Action repeat	4
Training steps	100k
Update	Distributional Q
Dueling	True
Support of Q-distribution	51
Discount factor $\gamma$	0.99
Batch size	32
Optimizer ( $\beta_1, \beta_2, \epsilon$ )	Adam (0.9, 0.999, 0.000015)
Learning rate	0.0001
Max gradient norm	10
Priority exponent	0.5
Priority correction	$0.4 \rightarrow 1$
EMA coefficient ( $\tau$ )	0.99
Exploration Network	Target
Exploration	Noisy nets
Noisy nets parameter	0.5
Replay buffer size	100k
Min buffer size for sampling	2000
Replay ratio	2
Multi-step return length	10
Q-head hidden units	512
Q-head non-linearity	ReLU
Evaluation trajectories	100
SAM parameter $\rho$	0.1
Reset interval	40,000

#### 7.4 Deepmind Control Suite Medium (DMC-M)

We utilized an open-source JAX implementation provided by Nikishin et al. [41] as the foundation for our work. We integrated the SAM optimizer implementation into this existing framework. To ensure consistency and comparability with prior studies, we strictly followed the architecture and hyperparameters outlined by Nikishin et al. [41], documented in Table 5.

In the case of the Base, L2, and Reset models described in Table 5, we adopted the results from Nikishin et al [41]. For the LN model, we incorporated layer normalization after each convolutional and fully-connected layer. Additionally, we replaced all ReLU activations with concatenated ReLU for the CReLU baseline.

We utilized the same training steps of 2,000,000 and reset interval of 100,000 for the DMC medium task as used by Nikishin et al [41].

Table 5: **Hyperparameters on DMC.** The ones introduced by this work are at the bottom.

Parameter	Setting
Gray-scaling	True
Observation down-sampling	(64, 64)
Frame stacked	3
Discount factor	0.99
Minibatch size	512
Learning rate	0.0003
Backbone: channels	32, 64, 128, 256
Backbone: stride	2, 2, 2, 2
Backbone: latent dim	50
Head: n. hidden layers	2
Head: hidden units	256
Target network update period	1
EMA coefficient $\tau$	0.995
Initial Temperature	0.1
Updates per step	1
Replay Buffer Size	1,000,000
Total training steps	2,000,000
Evaluation trajectories	100
SAM parameter $\rho$	Quadruped : 0.1 Others : 0.01
Reset interval	100,000

## 8 PseudoCode for applying SAM

### 8.1 Deep Q-Learning with SAM and Noisy Layers

We used the Rainbow agent and its variants to learn discrete control problems of the Atari-100k benchmark. Although there are many other components inside the Rainbow agent, such as multi-step learning, distributional RL, and dueling Deep Q-Network (DQN), it would be confusing to integrate all details together in the pseudocode. Thus, for simplicity of the display, we provide a pseudocode of applying SAM to one of the simplest baseline algorithms, vanilla DQN, in Algorithm 1. To elaborate more on the usage of noisy layers, we included such details in the pseudocode.

---

#### Algorithm 1: Deep Q-Learning with Noisy Layers & SAM

---

```

1 Input: Learning rate  $\eta$ ; SAM parameter  $\rho$ ; Replay ratio  $R$ ; Discount factor  $\gamma$ ; Polyak averaging
  factor  $\tau$ ;
2 Initialize: Replay memory  $\mathcal{D}$ ; Q-function weight  $w$ ; Target weight  $w^- \leftarrow w$ ;
3 foreach environment step  $t = 1, 2, \dots$  do
4   Collect a trajectory  $(s, a, r, s', d)$  with  $\varepsilon$ -greedy ( $d = \mathbb{1}[s'$  is terminal]);
5   Store the trajectory to  $\mathcal{D}$ ;
6   If  $d = 1$ , Reset environment state;
7   foreach optimization step  $i \in \{1, \dots, R\}$  do
8     Sample a minibatch of transitions  $\mathcal{B} = \{(s, a, r, s', d)\}$  from  $\mathcal{D}$ ;
9     Compute TD target  $y(r, s', d) = r + \gamma(1 - d) \max_{a'} Q_{w^-}(s', a')$ ;
10    // Perturbation step
11    Sample a random noise  $\xi$  of noisy layers inside Q-function;  $w \leftarrow w + \xi$ ;
12    Compute gradient  $g(w) = \nabla_w \frac{1}{|\mathcal{B}|} \sum_{(s,a,r,s',d) \in \mathcal{B}} (y(r, s', d) - Q_w(s, a))^2$ ;
13    Compute SAM perturbation  $\tilde{w}^{\text{SAM}} = w + \frac{\rho}{\|g(w)\|_2} g(w)$ ;
14    // Update step
15    Sample a random noise  $\xi'$  of noisy layers inside Q-function;  $\tilde{w}^{\text{SAM}} \leftarrow \tilde{w}^{\text{SAM}} + \xi'$ ;
16    Compute SAM gradient  $g^{\text{SAM}} = g(\tilde{w}^{\text{SAM}})$ ;
17    Gradient descent update  $w \leftarrow w - \eta g^{\text{SAM}}$ ; // Could be modified as any
    gradient-based optimizer
18    Update target weight  $w^- \leftarrow \tau w^- + (1 - \tau)w$ ;

```

---

## 8.2 Soft Actor-Critic with SAM

We also provide a pseudocode for applying SAM to the SAC algorithm. See Algorithm 2.

---

### Algorithm 2: Soft Actor-Critic with SAM

---

```

1 Input: Learning rates  $\eta_Q, \eta_\pi, \eta_\alpha$ ; SAM parameters  $\rho_Q, \rho_\pi, \rho_\alpha$ ; Replay ratio  $R$ ; discount factor
    $\gamma$ ; Polyak averaging factor  $\tau$ ; minimum expected entropy  $\mathcal{H}$ ;
2 Initialize: Replay memory  $\mathcal{D}$ ; Q-function weights  $w_1, w_2$ ; Q-function weights  $w_1^-, w_2^-$ ;
   Policy weight  $\theta$ ; Entropy regularization coefficient  $\alpha$ ;
3 foreach environment step  $t = 1, 2, \dots$  do
4   Observe state  $s$  and sample/execute an action  $a \sim \pi_\theta(\cdot|s)$ ;
5   Observe reward  $r$ , next state  $s'$ , and done signal  $d = \mathbb{1}[s' \text{ is terminal}]$ ;
6   Store the trajectory  $(s, a, r, s', d)$  to  $\mathcal{D}$ ;
7   If  $d = 1$ , Reset environment state;
8   foreach optimization step  $i \in \{1, \dots, R\}$  do
9     Sample a minibatch of transitions  $\mathcal{B} = \{(s, a, r, s', d)\}$  from  $\mathcal{D}$ ;
10    // Perturbation step
11    Compute target
        
$$y(r, s', d; \theta) = r + \gamma(1 - d) \left( \min_{i=1,2} Q_{w_i^-}(s', a') - \alpha \log \pi_\theta(a'|s') \right) \quad (a' \sim \pi_\theta(\cdot|s));$$

12    Compute Q-function gradient:
        
$$g_{Q,i}(w_i) = \nabla_{w_i} \frac{1}{|\mathcal{B}|} \sum_{(s,a,r,s',d) \in \mathcal{B}} (y(r, s', d; \theta) - Q_{w_i}(s, a))^2; \quad (i = 1, 2)$$

13    Compute policy gradient by sampling differentiable action  $\tilde{a}_\theta(s) \sim \pi_\theta(\cdot|s)$ :
        
$$g_\pi(w) = \nabla_\theta \frac{1}{|\mathcal{B}|} \sum_{s \in \mathcal{B}} \left( \min_{i=1,2} Q_{w_i}(s, \tilde{a}_\theta(s)) - \alpha \log \pi_\theta(\tilde{a}_\theta(s)|s) \right)^2;$$

14    Compute temperature gradient:  $g_{\text{temp}}(\alpha) = \nabla_\alpha \frac{1}{|\mathcal{B}|} \sum_{s \in \mathcal{B}} (-\alpha \log \pi_\theta(\tilde{a}_\theta(s)|s) - \alpha \mathcal{H})$ ;
        SAM-perturbations:
        
$$\begin{aligned} \tilde{w}_i^{\text{SAM}} &= w_i + \frac{\rho_Q}{\|g_{Q,i}(w_i)\|_2} g_{Q,i}(w_i); \quad (i = 1, 2) \\ \tilde{\theta}^{\text{SAM}} &= \theta + \frac{\rho_\pi}{\|g_\pi(\theta)\|_2} g_\pi(\theta); \\ \tilde{\alpha}^{\text{SAM}} &= \alpha + \frac{\rho_\alpha}{\|g_{\text{temp}}(\alpha)\|_2} g_{\text{temp}}(\alpha); \end{aligned}$$

15    // Update step
16    Compute target  $y(r, s', d; \tilde{\theta}^{\text{SAM}})$ ;
    Compute SAM gradients:
        
$$g_{Q,i}^{\text{SAM}} = g_{Q,i}(\tilde{w}_i^{\text{SAM}}), \quad g_\pi^{\text{SAM}} = g_\pi(\tilde{\theta}^{\text{SAM}}), \quad g_{\text{temp}}^{\text{SAM}} = g_{\text{temp}}(\tilde{\alpha}^{\text{SAM}});$$

17    Gradient descent updates:
        
$$w_i \leftarrow w_i - \eta_Q g_{Q,i}^{\text{SAM}}; \quad \theta \leftarrow \theta - \eta_\pi g_\pi^{\text{SAM}}; \quad \alpha \leftarrow \alpha - \eta_\alpha g_{\text{temp}}^{\text{SAM}};$$

        // Could be modified as any gradient-based optimizer
18    Update target weight  $w_i^- \leftarrow \tau w_i^- + (1 - \tau) w_i$ ;

```

---



## 9 Additional Ablation Studies

### 9.1 Experiments on SWA + Reset

Here we further investigate the efficacy of an optimization algorithm for better generalization capability. Specifically, we focus on Stochastic Weight Averaging (SWA) which also aims to find a flat minima of loss function [22]. SWA is an algorithm that takes a moving average periodically during training by storing a separate SWA weight  $w^{\text{SWA}}$  (other than the trained weight  $w$ ) and updating it as  $w^{\text{SWA}} \leftarrow \tau w^{\text{SWA}} + 1 - \tau w$  once per  $c$  updates of  $w$ . Note that SWA does not explicitly deviate the training trajectory; the only difference with vanilla training appears at evaluation time. Typically, SWA is not applied at the beginning of training but starts from some amount of vanilla training. In our application of SWA to RL, we applied averaging for the last 40K optimization steps with period  $c = 100$ , with the same base optimizer as our experiments on SAM.

We tested the harmonizing effect between SWA and resetting on the Atari-100k benchmark using the DrQ-Rainbow algorithm; the result is displayed in Table 6. Even though the performance due to SWA is better than the baseline, the enhancement is marginal. Specifically, the performance of SWA+Reset is not better than that of using Reset only (see Table 1). We surmise the reason for these marginal success/failure is that our RL agents already contains a similar module, a momentum target, accumulating a moving average of learned weights.

Table 6: **Performance of SWA on Atari-100k.** The results are averaged over 5 random seeds.

Algorithm	Method	Tr(F) ( $10^{-4}$ )	$\lambda_{\max}$	IQM	Median	Mean
DrQ	Base	5.54	16.07	0.258 (0.224, 0.292)	0.277 (0.209, 0.295)	0.476 (0.432, 0.520)
	SWA [22]	1.76	9.32	0.284 (0.252, 0.314)	0.278 (0.233, 0.312)	0.455 (0.415, 0.497)
	Reset [41]	6.44	26.62	0.343 (0.314, 0.373)	0.291 (0.231, 0.369)	0.660 (0.611, 0.715)
	SWA + Reset	1.90	11.02	0.332 (0.295, 0.374)	0.292 (0.234, 0.372)	0.645 (0.586, 0.709)

### 9.2 Further Ablations on the usage of SAM

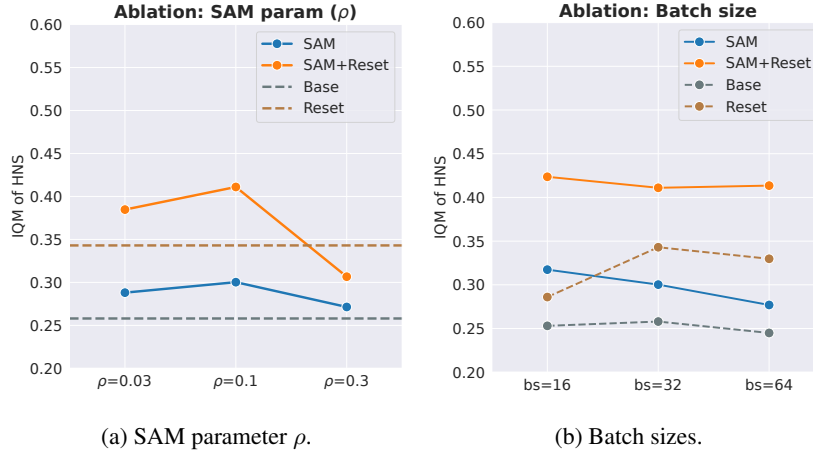


Figure 5: More ablation studies on using SAM.

**SAM parameter ( $\rho$ ).** Being the main hyperparameter of SAM, the  $\rho > 0$  represents the intensity of SAM perturbation. In every other experiment with DER and DrQ(-Rainbow), we do not tune the value of  $\rho$  but fix them as 0.1. Here, however, we run two other values of  $\rho$ 's, 0.03 and 0.3, to examine the effect of  $\rho$ . The result is shown in Figure 5a. We definitely observe the trade-off due to the size of  $\rho$ . If the  $\rho$  is too small, the scale of SAM perturbation becomes negligible and it cannot drastically improve the generalization capability compared to the case without SAM. However, a larger value of  $\rho$  is not always beneficial; the generalization capability does not always scale with the size of SAM perturbation. We, however, claim that finding an appropriate value of  $\rho$  is not too difficult; our recommendation is to test a few values between 0.01 and 1.

**Batch size.** We further study robustness with respect to batch sizes. We investigate the batch sizes among 16, 32 (baseline), and 64. From the resulting plot Figure 5b, we observe that SAM consistently improves the performance regardless of the choice of batch size, by comparing solid lines (SAM+Adam) and dashed lines (Adam). We also observe that the performance improvement between reset and non-reset becomes much larger when SAM is applied.

### 9.3 Increasing the Replay Ratio for SAM + Reset

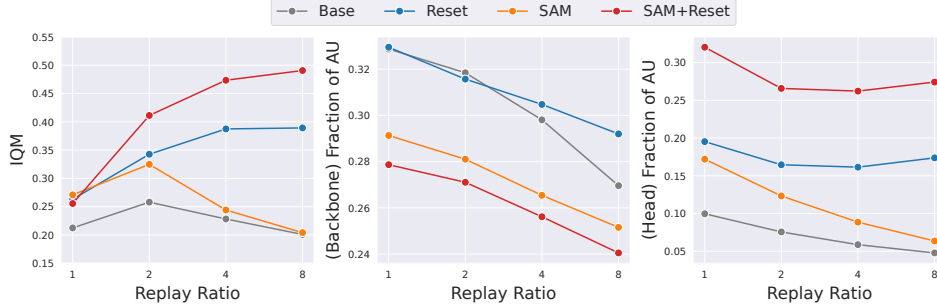


Figure 6: **Left.** Replay ratio scaling behavior of the methods in Atari-100k. **Middle & Right.** Percentile of the active units for backbone and head layers in various replay ratios.

Although increasing the number of updates per environment interaction (i.e., replay ratio) is critical for enhancing sample efficiency in reinforcement learning, simply increasing the replay ratio can lead to the loss of plasticity. In this section, we conduct an additional experiment to analyze whether the combined usage of SAM and Reset enhances the sample efficiency in a high replay ratio regime. We examine the performance of the SAM and Adam optimizers in conjunction with the DrQ algorithm using the Atari-100k benchmark.

As illustrated in Figure 6, the utilization of the SAM on the reset mechanism yields significant performance improvements, and these gains become more pronounced as the replay ratio increases. In the high replay rate setting, solely utilizing SAM exhibits a diminishing proportion of active units, which fails to prevent the loss of plasticity, resulting in performance degradation. Notably, the combined usage of SAM and Reset maintains a larger number of active units in the head network while simultaneously increasing sparsity in the backbone’s features. This combined usage effectively preserves plasticity and improves generalization, ultimately yielding the highest performance.

## 10 Per Environment Results

### 10.1 Atari-100k

Table 7: **Mean trajectory scores on State-of-the-art methods.** We report the individual scores on the 26 Atari games. For our methods, the results are averaged over 5 random seeds. For IRIS, DreamerV3, EfficientZero, and PlayVirtual, MLR, SR-SPR, the results are averaged over 5, 5, 32, and 15, 3, 10 seeds respectively.

Game	EfficientZero	IRIS	DreamerV3	PlayVirtual	MLR	SR-SPR:4	SR-SPR:8	SR-SPR:16	Ours:4	Ours:8
Alien	808.5	420.0	1095.8	947.8	990.1	964.4	1015.5	1107.8	1103.1	1115.9
Amidar	148.6	143.0	142.9	165.3	227.7	211.8	203.1	203.4	251.5	240.5
Assault	1263.1	1524.4	638.0	702.3	643.7	987.3	1069.5	1088.9	915.1	1104.5
Asterix	25557.8	853.6	982.8	933.3	883.7	894.2	916.5	903.1	952.8	1099.5
BankHeist	351.0	53.1	617.8	245.9	180.3	460.0	472.3	531.7	195.9	225.9
BattleZone	13871.2	13074.0	12800.0	13260.0	16080.0	17800.6	19398.4	17671.0	13624.0	21486.0
Boxing	52.7	70.1	67.8	38.3	26.4	42.0	46.7	45.8	44.0	44.8
Breakout	414.1	83.7	18.9	20.6	16.8	26.1	28.8	25.5	18.8	39.2
ChopperCommand	1117.3	1565.0	400.0	922.4	910.7	1933.7	2201.0	2362.1	863.2	662.0
CrazyClimber	83940.2	59324.2	71620.0	23176.7	24633.3	38341.7	43122.3	45544.1	28140.4	46710.8
DemonAttack	13003.9	2034.4	545.0	1131.7	854.6	3016.2	2898.1	2814.4	1967.3	2094.5
Freeway	21.8	31.1	0.0	16.1	30.2	24.5	24.9	25.4	29.9	30.4
Frostbite	296.3	259.1	1108.4	1984.7	2381.1	1809.9	1752.8	2584.8	2864.9	2242.0
Gopher	3260.3	2236.1	5828.6	684.3	822.3	717.5	711.2	712.4	737.4	569.0
Hero	9315.9	7037.4	10964.6	8597.5	7919.3	7195.7	7679.6	8524.0	7547.5	10115.5
Jamesbond	517.0	462.7	510.0	394.7	423.2	408.8	392.8	389.1	414.1	447.0
Kangaroo	724.1	838.2	3550.0	2384.7	8516.0	2024.1	3254.9	3631.7	3525.6	4905.4
Krull	5663.3	6616.4	8012.0	3880.7	3923.1	5364.3	5824.8	5914.4	5320.4	5951.1
KungFuMaster	30944.8	21759.8	29420.0	14259.0	10652.0	17656.5	17095.6	18649.4	19771.6	23209.8
MsPacman	1281.2	999.1	1388.5	1335.4	1481.3	1544.7	1522.6	1574.1	1678.2	1856.6
Pong	20.1	14.6	18.5	-3.0	4.9	-5.5	-3.0	2.9	-11.81	-1.7
Qbert	13781.9	745.7	3117.9	3620.1	3410.4	3699.8	3850.6	4044.1	3995.4	4779.3
RoadRunner	17751.3	9614.6	14036.6	13429.4	12049.7	14287.3	13623.5	13463.4	17804.4	14810.8
Seaquest	1100.2	661.3	582.0	532.9	628.3	766.6	800.5	819.0	721.9	742.8
PrivateEye	96.7	100.0	1124.0	93.9	100.0	95.8	95.8	97.9	100.0	76.2
UpNDown	17264.2	3546.2	9234.0	10225.2	6675.7	91435.2	95501.1	112450.3	42041.1	28954.8
IQM	<i>n/a</i>	0.501	0.497	0.374	0.432	0.544	0.589	0.632	0.510	0.625
Median	0.227	0.289	0.466	<i>n/a</i>	<i>n/a</i>	0.523	0.560	0.685	0.459	0.544
Mean	0.562	1.046	1.097	<i>n/a</i>	<i>n/a</i>	1.111	1.188	1.272	0.923	1.008
OG	<i>n/a</i>	0.512	0.505	0.558	0.522	0.470	0.452	0.433	0.486	0.442

Table 8: **Mean trajectory scores on DER algorithm.** We report the mean trajectory scores on the 26 Atari games, evaluated on top of DER. For each random seed, the results are averaged over 100 different trajectories at the end of training. The results are then averaged over 10 random seeds.

Game	Random	Human	Base	L2	SAM	LayerNorm	CReLU	Reset	SAM + Reset
Alien	227.8	7127.7	868.82	1067.2	810.68	717.28	703.04	962.48	963.04
Amidar	5.8	1719.5	147.41	194.94	172.16	152.57	145.98	150.19	191.49
Assault	222.4	742.0	380.04	493.69	399.88	355.65	396.5	430.02	526.68
Asterix	210.0	8503.3	710.4	822.4	624.8	475.2	731.3	681.88	691.1
BankHeist	14.2	753.1	77.74	63.1	53.26	83.74	57.2	106.59	74.26
BattleZone	2360.0	37187.5	9146.0	14308.0	11430.0	7988.0	7896.0	15951.25	15202.0
Boxing	0.1	12.1	-0.96	-1.14	-2.28	-2.59	-1.5	-0.62	-0.27
Breakout	1.7	30.5	4.7	2.67	4.42	5.46	5.37	6.45	7.81
ChopperCommand	811.0	7387.8	804.2	885.2	862.4	727.0	709.4	624.0	848.8
CrazyClimber	10780.5	35829.4	16350.8	23502.4	21498.2	16502.2	20216.2	20181.5	27968.4
DemonAttack	152.1	1971.0	340.11	519.86	354.41	300.09	382.5	428.86	390.7
Freeway	0.0	29.6	31.2	31.08	25.39	30.17	25.17	30.77	30.51
Frostbite	65.2	4334.7	970.94	2140.2	1402.44	1100.1	1436.88	1335.05	1982.02
Gopher	257.6	2412.5	273.0	381.56	348.28	414.32	312.44	384.27	484.68
Hero	1027.0	30826.4	8163.41	8799.29	6441.18	6702.81	7877.38	8033.26	7851.74
Jamesbond	29.0	302.8	280.8	463.7	279.9	285.9	298.4	314.56	427.6
Kangaroo	52.0	3035.0	2363.2	1079.6	2802.0	1006.0	1826.8	1869.12	1526.8
Krull	1598.0	2665.5	2997.52	2825.6	3181.96	3525.3	2852.1	3236.16	3547.26
KungFuMaster	258.5	22736.3	8923.6	15265.4	7359.4	5886.4	9618.2	16735.88	15311.6
MsPacman	307.3	6951.6	1342.22	1839.06	1578.06	1036.28	1048.36	1299.1	1597.7
Pong	-20.7	14.6	-16.39	-18.71	-12.62	-13.9	-11.95	-17.8	-12.13
Qbert	11.5	7845.0	3035.05	2288.55	3653.15	3505.25	2017.15	2731.69	3439.35
RoadRunner	68.4	42054.7	7062.4	11210.6	6799.6	2567.0	8158.8	11508.62	12368.4
Seaquest	24.9	69571.3	406.64	620.92	400.2	412.76	359.56	504.17	495.16
PrivateEye	163.9	13455.0	68.05	61.0	84.03	99.56	96.8	100.0	100.0
UpNDown	533.4	11693.2	3564.44	4612.74	3084.66	2536.62	3236.46	3863.95	4304.32
IQM	0.0	1.0	0.159	0.210	0.175	0.148	0.172	0.202	<b>0.252</b>
Median	0.0	1.0	0.175	0.216	0.210	0.171	0.149	0.179	<b>0.236</b>
Mean	0.0	1.0	0.298	0.375	0.313	0.262	0.294	0.366	<b>0.430</b>
OG	1.0	0.0	0.725	0.625	0.726	0.773	0.727	0.687	<b>0.644</b>

Table 9: **Mean trajectory scores on DrQ algorithm.** We report the mean trajectory scores on the 26 Atari games, evaluated on top of DrQ. For each random seed, the results are averaged over 100 different trajectories at the end of training. The results are then averaged over 10 random seeds.

Game	Random	Human	Base	L2	SAM	LayerNorm	CReLU	Reset	SAM + Reset
Alien	227.8	7127.7	757.62	789.38	854.84	899.14	1011.84	926.73	952.37
Amidar	5.8	1719.5	164.12	194.76	187.76	176.12	146.69	158.22	204.19
Assault	222.4	742.0	582.59	648.23	597.9	566.26	585.57	694.17	792.89
Asterix	210.0	8503.3	823.3	726.0	780.6	889.3	887.8	921.15	893.0
BankHeist	14.2	753.1	48.36	153.37	185.25	56.16	79.88	141.14	175.44
BattleZone	2360.0	37187.5	4088.0	2852.5	13999.0	14416.0	11306.0	4700.0	14327.0
Boxing	0.1	12.1	11.56	30.9	16.43	21.2	18.75	44.14	45.96
Breakout	1.7	30.5	13.16	13.06	12.64	13.71	10.56	18.46	18.83
ChopperCommand	811.0	7387.8	778.0	684.25	977.7	879.2	1150.6	777.5	804.8
CrazyClimber	10780.5	35829.4	13182.2	18933.0	17927.7	15852.8	13957.6	19082.8	19811.5
DemonAttack	152.1	1971.0	701.38	1137.11	735.54	556.33	531.05	1074.29	1530.96
Freeway	0.0	29.6	22.32	21.55	27.79	30.49	24.54	26.92	30.38
Frostbite	65.2	4334.7	1856.64	1731.48	2052.95	1409.34	763.64	1257.33	2096.56
Gopher	257.6	2412.5	374.28	547.35	476.02	433.92	445.88	711.14	675.18
Hero	1027.0	30826.4	5096.67	6578.28	6496.56	5645.98	6332.89	6987.43	6871.17
Jamesbond	29.0	302.8	348.8	422.75	333.3	287.2	239.7	369.2	410.4
Kangaroo	52.0	3035.0	3773.2	1930.75	3453.8	3589.0	4919.8	2830.8	1815.2
Krull	1598.0	2665.5	3612.06	3935.47	3385.05	3483.26	3710.24	4379.46	4734.11
KungFuMaster	258.5	22736.3	20412.4	9195.25	16380.3	8646.2	15188.4	12737.4	18800.9
MsPacman	307.3	6951.6	1210.02	1277.95	1471.33	1226.5	1191.2	1362.05	1486.02
Pong	-20.7	14.6	-8.82	-20.47	-6.42	-12.85	1.96	-10.0	-7.01
Qbert	11.5	7845.0	3776.3	2959.19	3495.45	2648.4	2429.2	3492.18	3564.98
RoadRunner	68.4	42054.7	15696.6	16391.25	11919.5	13045.6	13703.4	12939.5	14487.1
Seaquest	24.9	69571.3	525.88	661.5	519.2	394.24	383.8	645.26	706.12
PrivateEye	163.9	13455.0	100.0	75.0	96.04	100.0	99.4	100.13	100.0
UpNDown	533.4	11693.2	3690.74	10130.75	4963.46	5596.2	4565.04	15463.98	20130.01
IQM	0.0	1.0	0.258	0.271	0.325	0.259	0.256	0.343	<b>0.411</b>
Median	0.0	1.0	0.277	0.268	0.327	0.247	0.193	0.291	<b>0.374</b>
Mean	0.0	1.0	0.476	0.558	0.501	0.463	0.498	0.660	<b>0.753</b>
OG	1.0	0.0	0.633	0.631	0.589	0.627	0.628	0.579	<b>0.535</b>

## 10.2 DMC-M

Table 10: **Mean trajectory scores on DrQ algorithm.** We report the mean trajectory scores on the DMC medium environments, evaluated on top of DrQ. For each random seed, the results are averaged over 10 trajectories at the end of training. The results are then averaged over 10 random seeds.

Game	Base	L2	SAM	LayerNorm	CReLU	Reset	SAM + Reset
acrobot-swingup	16.34	14.87	15.36	23.45	40.79	57.83	61.40
cartpole-swingup_sparse	79.03	0.0	197.91	164.57	321.83	740.0	751.54
cheetah-run	727.44	694.97	736.61	591.47	835.33	665.67	636.53
finger-turn_easy	207.02	188.34	129.92	325.21	221.0	232.76	251.80
finger-turn_hard	80.95	59.51	60.07	485.70	117.5	89.11	181.87
hopper-hop	284.78	0.27	255.84	277.48	293.52	284.69	243.02
quadruped-run	155.06	73.18	261.03	266.84	78.89	466.93	438.67
quadruped-walk	88.08	72.22	130.85	173.13	80.02	632.33	683.96
reacher-easy	505.08	734.04	738.80	926.94	914.3	957.96	951.46
reacher-hard	450.96	462.64	495.32	746.55	795.77	794.53	766.37
walker-run	632.93	530.84	639.94	652.41	643.24	564.95	600.70
IQM	213	149	278	412	338	514	<b>519</b>
Median	288	238	341	415	398	491	<b>511</b>
Mean	293	257	332	421	394	498	<b>506</b>



## 11 Broader Impact

Our research possesses broader impacts in two different aspects. The first impact lies in the sample efficiency of Reinforcement Learning (RL) algorithms. We incorporate principles of generalizability and plasticity, leading to more efficient and adaptive solutions. This advance can improve RL's sample efficiency, opening new avenues for future research in this domain.

The second impact is on inclusivity and accessibility in RL. By decreasing data and computational demands, this work can aid underprivileged communities with fewer resources to participate in RL research and benefit from its many applications. This approach encourages a diverse range of perspectives and experiences in the field, enriching the community.

However, while our research has these positive implications, it is important to also acknowledge potential risks associated with RL technologies, particularly in robotics. We must continue to uphold ethical standards and prioritize safety to prevent misuse or harm that could arise from these advancements.